Published May 3, 2019

Original Research

Core Ideas

- Experiments measured saturation overshoot during infiltration of water into dry soil.
- Two models based on Richards' equation with a dynamic capillarity term simulated the data.
- The IFA model is an alternative approach to simulate saturation overshoot.
- The IFA model and dynamic capillarity equation were combined to simulate experiments.

Experimental and Numerical Studies of Saturation Overshoot during Infiltration into a Dry Soil

Luwen Zhuang,* S. Majid Hassanizadeh, C.J. van Duijn, Susanne Zimmermann, Irina Zizina, and Rainer Helmig

Downward infiltration of water into almost dry soil, when there is no ponding at the soil surface, often occurs in the form of fingers, with saturation overshoot at the finger tips. While this is well known, there is still uncertainty about the exact saturation pattern within fingers. We performed a series of one-dimensional water infiltration experiments into a dry soil to study the non-monotonicity of the saturation. We observed that saturation showed a non-monotonic behavior as a function of time. The overshoot was somewhat plateau shaped at relatively low flow rates but was quite sharp at higher flow rates. Two mathematical models, referred to as the extended standard (ESD) model and the interfacial area (IFA) model, were used to simulate the experimental results. Both models were based on extended forms of the Richards equation by including a dynamic capillary term. In the ESD model, standard equations for hysteresis were used. In the IFA model, the specific interfacial area was introduced to simulate hysteresis. Parameter values for both models were obtained from preliminary experiments or using empirical formulas. Only one parameter, the dynamic capillarity coefficient τ, was optimized to model saturation overshoot. While the ESD model did not reproduce the form of saturation overshoot for any combination of parameter values, the IFA model could provide good agreement with the data. To our knowledge, this is the first time where a combination of the IFA model and the dynamic capillarity equation has been used to simulate a set of experiments.

Abbreviations: ESD, extended standard; IFA, interfacial area.

L. Zhuang, S.M. Hassanizadeh, and C.J. van Duijn, Dep. of Earth Sciences, Utrecht Univ., Budapestlaan 4, P.O. Box 80021, 3508 TA, Utrecht, the Netherlands; S.M. Hassanizadeh, Soil and Groundwater Systems, Deltares, Princetonlaan 6, 3584 CB, Utrecht, the Netherlands; C.J. van Duijn, Dep. of Mechanical Engineering, Eindhoven Univ. of Technology, P.O. Box 513, 5600 MB, Eindhoven, the Netherlands; S. Zimmermann, Kleiststrasse 19, 70197, Stuttgart, Germany; I. Zizina and R. Helmig, Dep. of Hydromechanics and Modelling of Hydrosystems, Stuttgart Univ., Pfaffenwaldring 61, 70569, Stuttgart, Germany. *Corresponding author (luwen.zhuang@gmail.com).

Received 5 Sept. 2018.
Accepted 29 Jan. 2019.
Supplemental material online.

Citation: Zhuang, L., S.M. Hassanizadeh, C.J. van Duijn, S. Zimmermann, I. Zizina, and R. Helmig. 2019. Experimental and numerical studies of saturation overshoot during infiltration into a dry soil. Vadose Zone J. 18:180167. doi:10.2136/vzj2018.09.0167

Water infiltrating downward into a porous medium is known to often form wetting fingers instead of moving as a smooth front. Unstable fingering was observed first by Hill and Parlange (1972) for a layered soil. Later studies by Diment and Watson (1985) showed that unstable fronts also appear in non-layered dry soil. During the past several decades, many one-, two-, and three-dimensional experiments have been performed to investigate the mechanisms that could cause the appearance of fingers, including various factors that may affect their width and speed (Glass et al., 1989a; Liu et al., 1994a). Many experiments revealed a characteristic saturation overshoot at the tip of each finger (Selker et al., 1992; Liu et al., 1994a; Bauters et al., 2000; DiCarlo, 2004; Rezanezhad et al., 2006), as well as non-monotonic water pressure profiles (Stonestrom and Akstin, 1994; Geiger and Durnford, 2000; DiCarlo, 2007). In experiments by DiCarlo (2004), the saturation overshoot had a plateau form. However, the plateau was not observed in experiments by Rezanezhad et al. (2006) and Liu et al. (1994a), but rather a relatively sharp saturation overshoot. Hence, the question remains whether or not a plateau should be expected.

Early attempts to model gravitational fingers were based mostly on the classical form of the Richards equation (Glass et al., 1989b; Liu et al., 1994b; Nieber, 1996). These models, however, were not able to reproduce non-monotonic behavior (van Duijn et al., 2004; Egorov et al., 2003; Otto, 1997; Schweizer 2012). Various improvements and modifications have been proposed to extend the unsaturated flow model based on Darcy's law or the Darcy–Buckingham equation (e.g., Cueto-Felgueroso and Juanes, 2008; van Duijn et al., 2007; Egorov et al., 2002; Eliassi and Glass, 2002; Hilpert, 2012; Nieber et al.,

2003). Among these is the concept of dynamic capillarity proposed empirically by Stauffer (1978) and later described theoretically by Kalaydjian (1987) and Hassanizadeh and Gray (1990, 1993b). They showed that the difference in average fluid pressures is a function not only of saturation but also of the time rate of change in saturation. Such dynamic capillarity effects were already observed experimentally in the 1960s (e.g., Smiles et al., 1971; Topp and Peters, 1967). We refer to Hassanizadeh et al. (2002) for a review of experimental studies on dynamic effects. The extended Richards equation, with the dynamic capillary term included, has been studied mathematically by several researchers (e.g., Cao and Pop, 2016; Cuesta and Hulshof, 2003; van Duijn et al., 2013; Egorov et al., 2002). Numerical solutions of these models have been compared with experimental data by DiCarlo (2005) and Sander et al. (2008), among others. A detailed review of experimental and numerical studies of saturation overshoot can be found in Xiong (2014).

In addition to standard models that account for the effects of dynamic capillarity, an alternative formulation was proposed by Hassanizadeh and Gray (1990). Their model uses the specific interfacial area between the phases as an additional state variable. The full set of hysteretic capillary pressure–saturation curves (including all scanning curves) is then replaced by a single interfacial area–capillary pressure–saturation surface. The existence of such a surface has been shown using computational pore-scale models (cf., Held and Celia, 2001; Joekar-Niasar et al., 2008; Joekar-Niasar and Hassanizadeh, 2012; Reeves and Celia, 1996), as well as experimentally (Chen and Kibbey, 2006; Chen et al., 2007; Karadimitriou et al., 2014). The interfacial area model has been used to simulate several hypothetical problems (Niessner and Hassanizadeh, 2008, 2009a, 2009b; Pop et al., 2009; Landa-Marbán et al., 2017). Unfortunately, many uncertainties still exist about the model. For example, it is not clear what the importance of various terms are and how the various material coefficients should be determined experimentally. Also, to our knowledge, only two studies exist where the interfacial area model has been used to simulate experiments (Zhuang et al., 2016, 2017b). These two studies were both related to horizontal redistribution, which has a flow regime and experimental design that is very different from downward water infiltration studies. In particular, in horizontal moisture redistribution, the flow is typically very slow and the effects of dynamic capillarity are expected to be negligible. No studies have been reported thus far on the simulation of experiments using the interfacial area model while accounting for the effects of dynamic capillarity.

For this study, we first performed a series of one-dimensional downward infiltration experiments in a relatively dry soil. The experiments were conducted at six different flow rates and different initial saturations. Saturation was measured at one location using the γ-transmission method. We used two alternative approaches, referred to as the extended-standard (ESD) model and the interfacial area (IFA) model, to simulate the experimental results. Both models are based on modified forms of the classical Richards equation by adding a dynamic capillarity term. The main difference between the two models is the manner in which hysteresis is modeled. For the ESD model, we used relatively standard formulations for hysteresis in the capillary pressure and relative permeability curves. For the IFA model, hysteresis was modeled by introducing the specific interfacial area as an additional state variable. Capillary pressure and saturation are then treated as independent variables, while the interfacial area is assumed to be a unique function of capillary pressure and saturation. Also, the relative permeability is then assumed to be a function of the interfacial area as well as saturation. We performed a series of sensitivity analyses to determine the effect of various parameters on the magnitude and extent of saturation overshoot.

Here, we first briefly summarize the ESD and IFA models and describe the experiments. We then compare computational results with the experimental data.

Mathematical Models

First, we present common elements of the two models, namely, the Richards equation and the dynamic capillarity equation. This is followed by a brief description of how hysteresis is accounted for in the ESD and IFA models.

Main Governing Equations

One-Dimensional Richards Equation

The mass balance equation for the water phase combined with the Darcy–Buckingham law is usually considered to model multiphase flow in porous media. Known as the Richards equation, in one-dimensional form, the resulting model can be written as

$$\phi\frac{\partial S^{\mathrm{w}}}{\partial t}+\frac{\partial}{\partial x}\left[-\frac{k^{\mathrm{rw}}\left(S^{\mathrm{w}}\right)k}{\mu^{\mathrm{w}}}\left(\frac{\partial p^{\mathrm{w}}}{\partial x}-\rho^{\mathrm{w}}g\right)\right]=0 \qquad [1]$$

where the superscript w represents the water phase, ϕ is porosity, S^{w} (dimensionless) is water saturation (water content divided by porosity), μ^{w} [M L^{-1} T] is the viscosity of water, ρ^{w} [M L^{-3}] is the density, g [L T^{-2}] is gravity, p^{w} [M L^{-1} T^{2}] is water pressure, k^{rw} (dimensionless) and k [L^{2}] denote relative and intrinsic permeabilities, respectively, t [T] is time, and x [L] is the vertical coordinate (positive here in the downward direction).

Dynamic Capillarity Equation

In classical soil sciences, the difference between air and water pressures is considered to be equal to the capillary pressure and is given as a function of saturation. The air pressure is commonly assumed to be constant throughout the modeling domain. Then, taking air pressure as the reference pressure, the capillary pressure–saturation relationship is usually written as $p^{\mathrm{w}}=p^{\mathrm{c}}(S^{\mathrm{w}})$. In this study, however, we replace this expression by a so-called dynamic capillarity relationship. A linear approximation for this relationship is given by (Hassanizadeh and Gray, 1993a; Hassanizadeh et al., 2002)

$$-p^{\mathrm{w}}=p^{\mathrm{c}}\left(S^{\mathrm{w}}\right)-\tau\frac{\partial S^{\mathrm{w}}}{\partial t} \qquad [2]$$

where p^c [M L^{-1} T^2] is the capillary pressure, and τ [M L^{-1} T] is the dynamic capillarity coefficient. Many studies have shown that τ may be a function of saturation (O'Carroll et al., 2005; Manthey et al., 2008; Joekar-Niasar and Hassanizadeh, 2011b; Bottero et al., 2011; Diamantopoulos and Durner, 2012; Abidoye and Das, 2014; Goel et al., 2016). Furthermore, the relationship between τ and saturation was found to be nonunique for imbibition and drainage processes (Das and Mirzaei, 2012; Zhuang et al., 2017a). Also, the dependence between capillary pressure and saturation is known to be hysteretic, as described below.

Hysteresis

The Extended-Standard Model

Equations [1] and [2] for the ESD model must be completed with a full set of hysteretic capillary pressure–saturation relationships. Also, the relative permeability–saturation relationship is, in principle, hysteretic. For the basic formulas, we used the van Genuchten–Mualem equations (van Genuchten, 1980; Luckner et al., 1989):

$$p^c\left(S^w\right)=\frac{1}{\alpha}\left(S_e^{-1/m}-1\right)^{1/n} \quad 0\le S_e\le 1 \qquad [3]$$

$$k^{rw}\left(S^w\right)=\left(S_e\right)^{l}\left[1-\left(1-S_e^{1/m}\right)^{m}\right]^2 \quad 0\le S_e\le 1 \qquad [4]$$

$$S_e=\frac{S^w-S_{ir}^w}{1-S_{ir}^w-S_r^a} \qquad [5]$$

where $S_{ir}{}^w$, $S_r{}^a$, and S_e (all dimensionless) are irreducible water saturation (the volume of entrapped water divided by porosity), residual air saturation (the volume of entrapped air divided by porosity), and effective water saturation, respectively, α [L^{-1}] and n (dimensionless) are quasi-empirical parameters, $m = 1 - 1/n$, and l (dimensionless) was set equal to 0.5 for most simulations. Relationships for the main drainage curves, denoted by $p_{dr}{}^c$ and $k_{dr}{}^{rw}$, were obtained by using the values of α and n for main drainage in Eq. [3] and [4]. Similarly, the curves for $p_{im}{}^c$ and $k_{im}{}^{rw}$ were obtained by inserting corresponding values of α and n for primary imbibition in Eq. [3] and [4]. The value of the irreducible water saturation, $S_{ir}{}^w$, for primary imbibition was zero.

Different approximate formulations have been used for the scanning curves (cf., Kool and Parker, 1987; Parker and Lenhard, 1987). In addition to the Kool–Parker model, we used in this study also a play-type hysteresis model (van Duijn et al., 2018; Beliaev and Hassanizadeh, 2001; Rätz and Schweizer, 2014) for both the relative permeability and the capillary pressure curves. For the play-type hysteresis model, we used (Rätz and Schweizer, 2014)

$$k^{rw}=\frac{k_{im}^{rw}+k_{dr}^{rw}}{2}+\frac{k_{im}^{rw}-k_{dr}^{rw}}{2}\operatorname{sign}\left(\frac{\partial S^w}{\partial t}\right) \qquad [6]$$

$$p^c=\frac{p_{im}^c+p_{dr}^c}{2}+\frac{p_{im}^c-p_{dr}^c}{2}\operatorname{sign}\left(\frac{\partial S^w}{\partial t}\right) \qquad [7]$$

where

$$\operatorname{sign}\left(\frac{\partial S^w}{\partial t}\right)=\begin{cases}1 & \text{when } \dfrac{\partial S^w}{\partial t}>0\\ -1 & \text{when } \dfrac{\partial S^w}{\partial t}<0\end{cases} \qquad [8]$$

For numerical convenience, we replaced Eq. [8] by the smooth function $H_\varepsilon(\partial S^w/\partial t)$ defined as

$$H_\varepsilon\left(\frac{\partial S^w}{\partial t}\right)=\frac{2}{\pi}\arctan\left(\frac{1}{\varepsilon}\frac{\partial S^w}{\partial t}\right) \qquad [9]$$

where ε is a small parameter that controls the manner in which H_ε approximates the sign function. (Note that the sign and H_ε functions have no physical dimensions, while the small parameter ε has unit s^{-1}). Using H_ε in Eq. [6] and [7] implies that k^{rw} and p^c vary continuously from imbibition to drainage (and vice versa) when the saturation time derivative reverses.

When solving the full set of equations in the ESD model, the value of effective saturation is not constrained. Large τ values may lead to large overshoots, with saturation exceeding $1 - S_r{}^a$. This means that S_e then could become larger than unity, in which case Eq. [3] and [4] are undefined, since $1/n \in (0,1)$ and $m = 1 - 1/n \in (0,1)$. To have well-defined p^c and k^{rw} also for $S_e > 1$, we complemented Eq. [3] and [4] with the following extension for possible values of $S_e > 1$ (van Duijn et al., 2018):

$$\begin{cases}p^c\left(S^w\right)=\dfrac{1}{\alpha^*\varepsilon_d}\left(1-S_r^a-S^w\right) & S_e>1\\ k^{rw}=1 & S_e>1\end{cases} \qquad [10]$$

Here, the value of the α^* was chosen to be the arithmetic mean of α values for drainage and imbibition. The parameter ε_d is dimensionless, positive, and needs to be small. This will ensure that water saturation S^w may exceed $1 - S_r{}^a$ only slightly. In fact, van Duijn et al. (2018) showed that in the limit when $\varepsilon_d \to 0$, water saturation remains bounded by $1 - S_r{}^a$. We have given ε_d the value $\varepsilon_d = \varepsilon t_{ref}$, where t_{ref} is a characteristic reference time. Throughout this study, the dimensional parameter ε in Eq. [9] was chosen such that ε_d was on the order 10^{-4} to 10^{-3}. In the ESD model, the governing differential equations are hence Eq. [1] and [2], combined with auxiliary Eq. [3–10].

The Interfacial Area Model

In the traditional theory of unsaturated flow in porous media, water saturation and pressure are the only state variables. In other words, it is assumed that knowing them is sufficient for characterizing unsaturated flow under all conditions (drainage and imbibition), and capillary pressure is assumed to be a function of saturation only. Many studies, however, have shown that pressure and saturation are not sufficient for uniquely defining the state of the system (see Hassanizadeh, 2015). There is a new class of porous media models wherein a third state variable, namely the air–water specific interfacial area, is introduced to provide a sufficient description of unsaturated flow processes (see, e.g., Joekar-Niasar

and Hassanizadeh, 2011a). This new variable, denoted by a^{wa} [L^{-1}], is defined as the amount of air–water interfacial area per unit volume of the porous medium.

For the IFA model, we still use Eq. [1] and [2]. However, Eq. [3–10] for capillary pressure and relative permeability, given above, are replaced by a new constitutive equation for the air–water specific interfacial area (Hassanizadeh and Gray, 1990, 1993b). Indeed, several studies have shown that each equilibrium p^c–S^w point (primary, main, or scanning) corresponds to a point on a unique p^c–S^w–a^{wa} surface (e.g., Chen and Kibbey, 2006; Joekar-Niasar and Hassanizadeh, 2012, 2011a; Karadimitriou et al., 2014). This means that p^c–S^w loops correspond to paths on the three-dimensional p^c–S^w–a^{wa} surface projected on the p^c–S^w plane. Similarly, the hysteretic relationship between relative permeability (k^{rw}) and saturation (S^w) can be replaced by a unique k^{rw}–S^w–a^{wa} surface (Joekar-Niasar et al., 2008).

Because no experimental data were available for the specific interfacial area for the sand used in this study, we used a numerical approach proposed by Bradford and Leij (1997) to generate the p^c–S^w–a^{wa} surface. A similar method was used to generate the k^{rw}–S^w–a^{wa} surface. Details are given in Appendix A. For the p^c–S^w–a^{wa} surface, we used the following formula proposed by Joekar-Niasar and Hassanizadeh (2012):

$$a^{wa}\left(S^w, p^c\right) = \gamma_1 S^w \left(1 - S^w\right)^{\gamma_2} \left(\alpha p^c\right)^{\gamma_3} \quad [11]$$

where γ_1, γ_2, and γ_3 are fitting parameters, and the superscript *wa* represents water and air. The parameter α is the same as in the van Genuchten–Mualem model and is used here to make the last term on the right-hand side dimensionless. We used for our analysis the value of α for the primary imbibition curve.

For the k^{rw}–S^w–a^{wa} surface, the following formula was used:

$$k^{rw}\left(S^w, a^{wa}\right) = S^{w\left(-\lambda_1 a^{wa} + \lambda_2\right)} \quad [12]$$

where λ_1 and λ_2 are fitting parameters. Equation [12] was based on the Brooks–Corey–Burdine equation for k^{rw} (Brooks and Corey, 1964), which is a simple power function of saturation, with the value of the exponent being different for drainage and imbibition. In Eq. [12], different values of the specific interfacial area (a^{wa}) during imbibition and drainage result in different values of the exponent for different paths.

For the air–water specific interfacial area, an evolution equation must be provided. Assuming that the air–water interfacial mass density is constant, the following equation can be used (Hassanizadeh, 2015):

$$\frac{\partial a^{wa}}{\partial t} + \frac{\partial\left(a^{wa} w^{wa}\right)}{\partial x} = E^{wa} \quad [13]$$

where w^{wa} is the macroscopic flux of the specific interfacial area, given by a Darcy-type equation (Hassanizadeh, 2015):

$$w^{wa} = -k^{wa}\left(\frac{\partial a^{wa}}{\partial x} + \Omega \frac{\partial S^w}{\partial x}\right) \quad [14]$$

in which k^{wa} is the interfacial permeability, including surface tension, and Ω is a material coefficient. The term E^{wa} accounts for the net production rate of the specific interfacial area, for which the following approximation was developed by Zhuang et al. (2016):

$$E^{wa} = -L \frac{\partial a^{wa}}{\partial p^c} \frac{\partial S^w}{\partial t} \quad [15]$$

where L is a material coefficient that may depend on a^{wa} and S^w.

Recent numerical and experimental studies by Joekar-Niasar and Hassanizadeh (2011a) and Karadimitriou et al. (2014) have shown that the value of the interfacial permeability coefficient is very small. As a result, w^{wa} and the corresponding term in Eq. [13] can be disregarded. Thus, combining Eq. [13] and [15] reduces then to

$$\frac{\partial a^{wa}}{\partial t} = -L \frac{\partial a^{wa}}{\partial p^c} \frac{\partial S^w}{\partial t} \quad [16]$$

Substituting Eq. [11] into [16] allows us to eliminate $\partial a^{wa}/\partial t$ from Eq. [16]. As a result, a relationship between $\partial p^c/\partial t$ and $\partial S^w/\partial t$ is obtained. That relationship can be integrated for a constant L and a given set of initial conditions [$p_0{}^c(x)$, $S_0{}^w(x)$]. The result is a unique and invariant (i.e., non-hysteretic) relation between p^c and S^w at each given point in space (see Pop et al. [2009], for the derivation). The IFA model given by Eq. [1], [2], [11], and [16] is hence not able to handle hysteretic behavior.

To introduce hysteresis into the model, we propose to give the production parameter L in Eq. [16] different values for drainage and imbibition. Hence we propose to use

$$L = \frac{L_{im} + L_{dr}}{2} + \frac{L_{im} - L_{dr}}{2} H_\varepsilon\left(\frac{\partial S^w}{\partial t}\right) \quad [17]$$

where L_{im} and L_{dr} are the values of L for imbibition and drainage, respectively. Values for L_{im} and L_{dr} were obtained by fitting the experimental infiltration data. In summary, the IFA model consists of Eq. [1], [2] and [16], combined with auxiliary Eq. [11], [12], and [17].

Comparison of Models

The IFA model is a relatively new model. One of its most appealing features is that it is more physically based. The coefficient L is related to the production rate of the area of air–water interfaces. Given the fact that water invades small pores first during imbibition and first drains from large pores during drainage, it is physically reasonable to have different values for different imbibition and drainage processes. Any coefficient (even porosity or permeability) is obtained by fitting experimental data. In principle, the coefficient L should be determined experimentally for each soil type. In fact, the coefficient L can be a function of saturation and interfacial area. Because currently there exists little information about this coefficient, we simulated the dependence of L by prescribing it to be different for imbibition and drainage, denoted as two constant parameters L_{im} and L_{dr}, respectively. The values were chosen so that simulation results fit the transient data. The important point is not to change the value of the parameter

each time the conditions change. In our study, once the values of L_{im} and L_{dr} were optimized based on one experiment, they were fixed for other experiments. The values of L were not fitted for each new experiment. Therefore, there is only one fitting parameter τ in both the IFA model and the ESD model. Note that had we introduced different scanning curves in the ESD model, then additional parameters would have been needed there, too.

Description of Experiments

Selected Sand

We performed a number of experiments involving three different sand types: two coarse sands and one medium-grained sand. More details can be found in Fritz (2012). Here we report results for only the coarse sand. The sand was obtained from a riverbed and had particle diameters ranging from 0.57 to 1.05 mm, with d_{50} = 0.79 mm. The sand was washed thoroughly with deionized water and then oven dried prior to use. The saturated hydraulic conductivity was measured using the constant-head method, giving an average value of 5.61×10^{-3} m s^{-1}. The capillary pressure–saturation curves were measured using the multistep hanging water column method. Figure 1 shows the measured primary imbibition and main drainage curves, and the fitted curves using the van Genuchten Eq. [3]. We have summarized all hydraulic parameters in Table 1. The k^{rw}–S^w–a^{wa} and p^c–S^w–a^{wa} surfaces of the sand are shown in Fig. 2. Appendix A summarizes how they were obtained. The final set of parameters used in Eq. [11] and [12] are listed in Table 2.

Experimental Setup

We performed a series of quasi one-dimensional experiments in acrylic plastic tubes uniformly filled with sand. The column dimensions were 50 cm in length and 1 cm in diameter. A schematic view of the setup is shown in Fig. 3, including the location of several pressure transducers along the column. Teflon grease was applied to the inner surface of the column. Some studies have shown that an air pressure gradient may cause fingering flow in a closed porous media system (Jury et al., 2003; Fürst et al., 2009; Wang et al., 1998, 2004). To avoid an air pressure gradient in our system, water was sprinkled on the sand surface at a pre-specified constant flow rate using a peristaltic pump. A hydrophilic membrane on the top of the sand was used to establish spatially uniform inflow. A small gap between the wall of the setup and the membrane caused the air pressure at the inlet to remain atmospheric. The bottom of the column was open to air.

We performed the experiments at six different constant inflow rates, ranging from 7.5×10^{-6} to 5×10^{-4} m s^{-1}, combined with three different values of initial saturation: 0.00, 0.03, and 0.10. For experiments that had zero initial water saturation, air-dried sand was packed uniformly into the column. For experiments that had initial saturations of 0.03 or 0.10, we followed a special procedure to have the sand wetted as uniformly as possible. Dry sand was first mixed with a certain amount of deionized and degassed water to obtain an approximate pre-specified saturation. We then placed the wet sand into a large air-tight container, which was kept overnight in an oven at 50°C. This would cause the water to evaporate and fill the pores uniformly. Subsequent cooling of the container to room temperature would allow the water vapor to condensate and wet the sand uniformly. Once placed into the acrylic plastic columns, saturation during the ensuing experiments was measured at 20 cm below the inlet every 20 s using a dual-energy γ-ray system. A measurement interval of 20 s was used as determined by the measured accuracy of the γ-ray system. Detailed information can be found in Appendix B. Other details about the γ-ray system and the γ transmission method were given by Fritz (2012) and Zhuang et al. (2017a). All experiments were conducted in a constant-temperature room (21 ± 0.5°C).

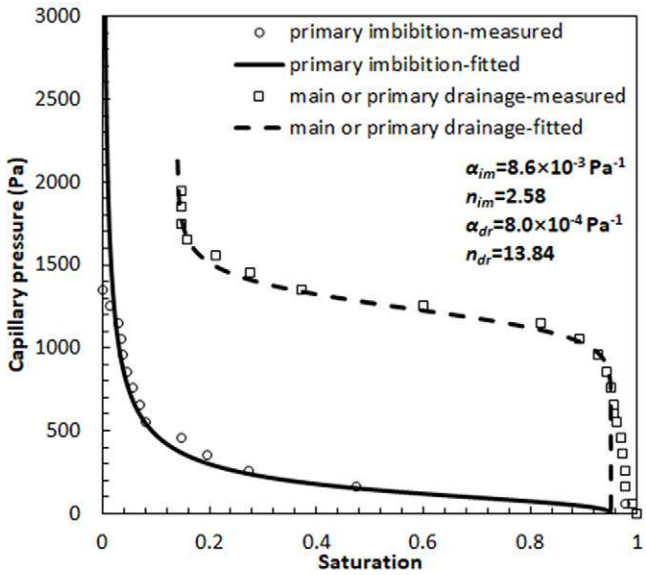

Fig. 1. Measured and fitted van Genuchten primary imbibition and main drainage curves using the van Genuchten parameters for imbibition (α_{im} and n_{im}) and drainage (α_{dr} and n_{dr}).

Results and Discussion

Experimental Results

Figure 4 presents water saturation breakthrough curves measured at a fixed distance (x = 20 cm). The plot on the left

Table 1. Measured soil properties and parameter values

Parameter	Value
Average porosity (ϕ)	0.4
Water density (ρ^w), kg m^{-3}	1×10^3
Water viscosity (μ^w), Pa s	1×10^{-3}
Intrinsic permeability (k), m^2	6.43×10^{-10}
Main drainage retention exponent n	13.84
Main drainage retention parameter α, Pa^{-1}	8.0×10^{-4}
Primary imbibition retention exponent n	2.58
Primary imbibition retention parameter α (Pa^{-1})	8.6×10^{-3}
Irreducible water saturation (S_{ir}^w)	0.14
Residual air saturation (S_r^a)	0.05

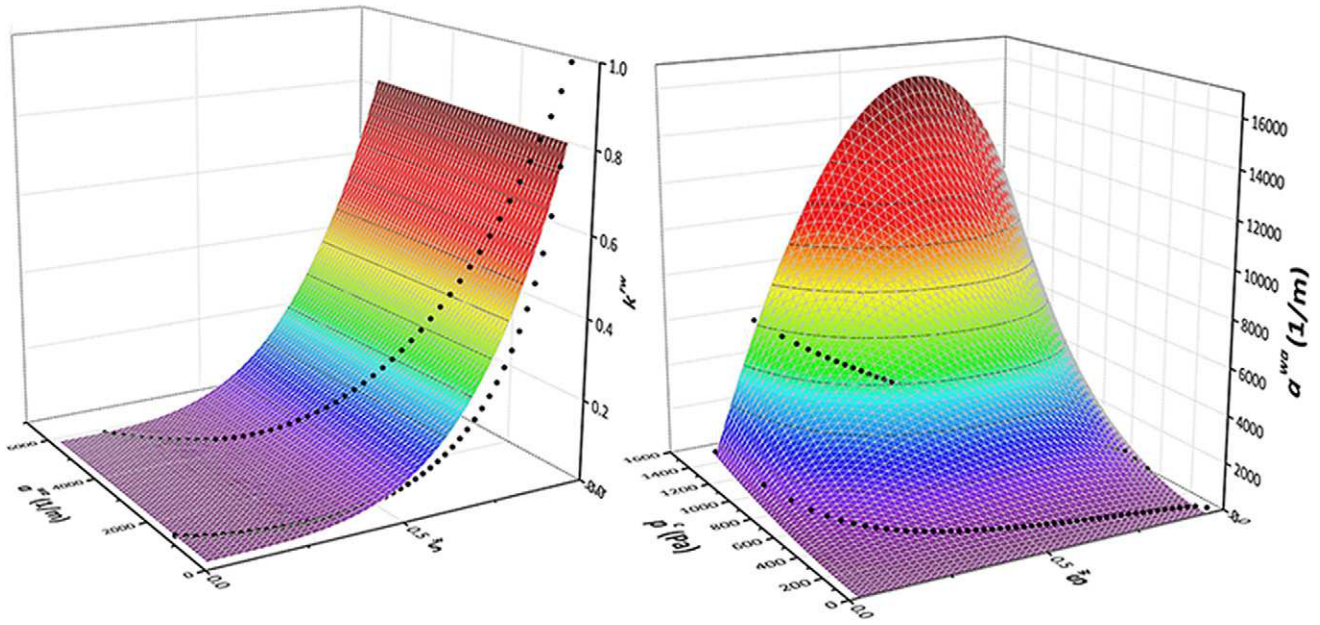

Fig. 2. Three-dimensional relative permeability (k^{rw})–water saturation (S^w)–air–water specific interfacial area (a^{wa}) surface (left) and capillary pressure (p^c)–S^w–a^{wa} surface (right). The black dots represent k^{rw}–S^w–a^{wa} (left) and p^c–S^w–a^{wa} (right) points obtained using the method described in Appendix A.

(Fig. 4a) shows results for six different inflow rates at zero initial saturation, and the plot on the right (Fig. 4b) shows results for three different initial values of saturation at an inflow rate of 4.3×10^{-5} m s^{-1}. Note that saturation overshoot occurred for all selected flow rates when the soil was initially dry. Moreover, the duration of the overshoot increased, and its magnitude decreased slightly, with decreasing flow rate. Saturation overshoot at the low flow rates (1.7×10^{-5} and 7.5×10^{-6} m s^{-1}) followed a decreasing plateau-shaped curve but not at the higher flow rates. Furthermore, at a fixed flow rate, the height of the overshoot decreased with increasing initial water saturation. No overshoot occurred for the initial saturation of 0.10, which is close to the irreducible water saturation (see Table 1).

DiCarlo (2004) observed a sharp overshoot at relatively low flow rates but a plateau-shaped overshoot at higher flow rates. However, contrary to DiCarlo's study, we observed a plateau-shaped overshoot only for very small flow rates. We note that we may not have captured some small peaks with our measurement interval of 20 s, but they would not have changed the overall shape of the saturation overshoot.

Table 2. Values of the coefficients in Eq. [11] and [12].

Parameter	Value	SD
γ_1, m^{-1}	582	21
γ_2	0.7	0.05
γ_3	1.9	0.02
Goodness of fit, Eq. [11]	0.95	
λ_1, m	7.0×10^{-5}	6.7×10^{-6}
λ_2	4.0	0.14
Goodness of fit, Eq. [12]	0.90	

Numerical Results

Model Parameters, Initial and Boundary Conditions

Most parameters needed for the ESD model were measured directly (notably porosity and intrinsic permeability) or obtained by fitting capillary pressure–saturation curves, which were also

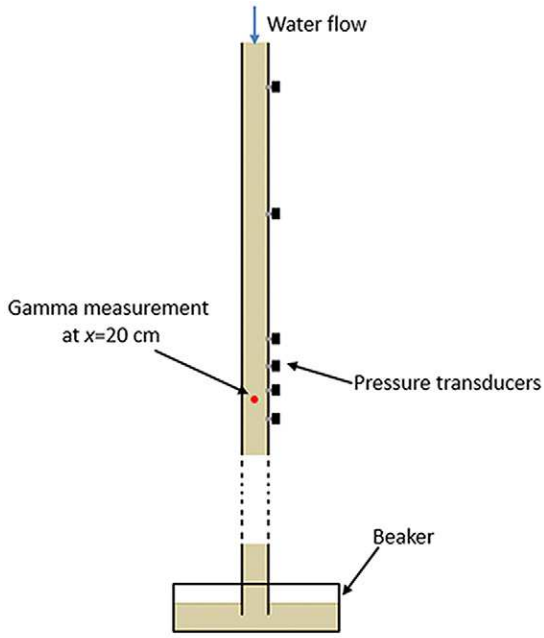

Fig. 3. Schematic view of the experimental setup.

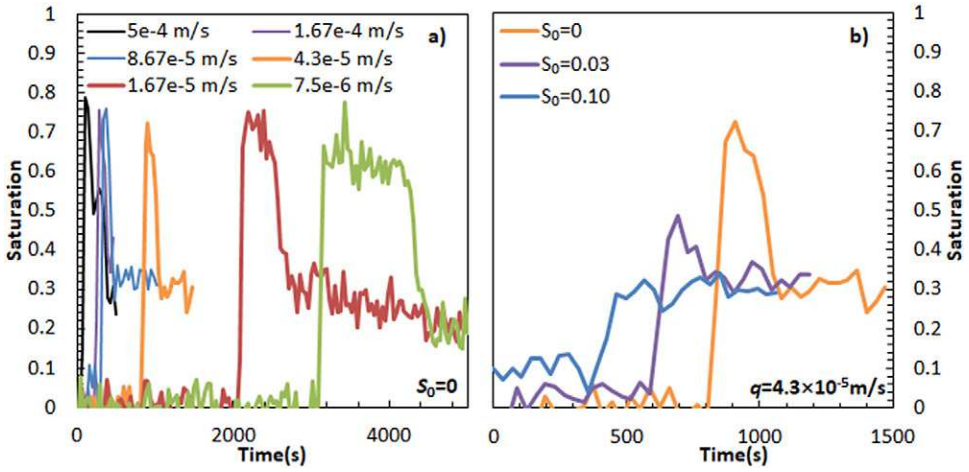

Fig. 4. Measured saturation breakthrough curves at 20 cm (a) in the initially dry soil for different flow rates and (b) at different initial saturations (S_0) at a fixed flow rate (q) of 4.3×10^{-5} m s^{-1}.

measured. The parameters are given in Table 1. The only parameter obtained by fitting the saturation overshoot experiments was the dynamic capillarity coefficient τ. For the IFA model, in addition to porosity and permeability as given in Table 1, we determined the parameters of the p^c–S^w–a^{wa} and k^{rw}–S^w–a^{wa} surfaces for the sand a priori using empirical formulas (Eq. [11] and [12]). The resulting parameters are given in Table 2. Three parameters had been obtained by fitting saturation overshoot experiments: the dynamic capillarity coefficient τ and the interfacial area production term coefficients L_{im} and L_{dr} in Eq. [17]. Best-fit values of these parameters are given in Table 3.

The equations in the ESD and IFA models were solved using the commercial simulation package COMSOL Multiphysics 5.0 (COMSOL, 2014). From preliminary simulations, we determined that a grid size of 1×10^{-4} m and a maximum time step of 0.1 s would give us mesh-independent solutions. A convergence tolerance of 1×10^{-8} was used to achieve accurate solutions. The modeling domain was 0.5 m long. Initial conditions were set to the initial saturations in the column (0.00, 0.03, or 0.10). For the initially dry sand simulation, we used a very small value of 0.01 as the initial saturation to avoid singular behavior of the pressure. The boundary conditions were

$$q = q_0 \text{ at } x = 0 \quad [18]$$

$$S = S_0 \text{ at } x = L \quad [19]$$

Because saturation and capillary pressure are treated as independent variables in the IFA model, an extra set of initial and boundary conditions is needed. These were chosen as

$$\frac{\partial a^{wa}}{\partial x} = 0 \text{ at } x = 0 \quad [20]$$

$$p^c = p^c_{im}(S_0) \text{ at } x = L \quad [21]$$

By virtue of Eq. [11], Eq. [20] is converted to a mixed boundary condition for S^w and p^c. The initial value of capillary pressure was chosen from the primary imbibition curve corresponding to the initial saturation. For all numerical simulations, we used the calculated saturation breakthrough curves at 20 cm to provide comparisons with the experimental data.

Sensitivity Analysis

First, we performed a sensitivity analysis of the ESD model (i.e., of the one-dimensional Richards equation with dynamic capillarity effects but no capillary hysteresis), to investigate the effects of various parameters. The parameters we considered were the dynamic capillarity coefficient τ, the exponent l in Eq. [4] for the relative permeability, and initial saturation. Values of the parameters α and n for primary imbibition were kept constant. We compared the results mainly in terms of two aspects: the shape (width and height) of saturation overshoot and the arrival time of the moisture front. Results of the sensitivity analysis are presented in Fig. 5.

As can be seen in Fig. 5a, the dynamic capillarity coefficient τ has a strong effect on the shape and arrival time of saturation overshoot. As expected, a monotonic front was found for $\tau = 0$. The conventional equilibrium theory of capillarity is evidently not able to capture the observed non-monotonic saturation behavior, thus echoing previous mathematical analyses and numerical studies. Increasing the value of τ leads to more extensive overshoot and a delay in the arrival time (see Fig. 5a). The inflow rate and initial saturation also impact the non-monotonicity. This is evident from

Table 3. Best-fit parameter values in the extended-standard (ESD) and interfacial area (IFA) models for the different experiments (S_0, initial saturation; τ, dynamic capillarity coefficient; L_{im} and L_{dr}, defined in Eq. [17]).

Experimental conditions		ESD model	IFA model			
Flow rate	S_0	τ	Flow rate adjusted by	τ	L_{im}	L_{dr}
m s^{-1}		Pa s	%	Pa s	Pa	
4.30×10^{-5}	0	1×10^4	−7	1.3×10^4	390	1300
1.67×10^{-5}	0	6×10^4	−7	1×10^5	390	1300
7.50×10^{-6}	0	1.4×10^5	0	2.5×10^5	390	1300
4.30×10^{-5}	0.03	8×10^3	−7	1×10^4	390	1300
4.30×10^{-5}	0.10	1×10^3	0	1×10^3	390	1300

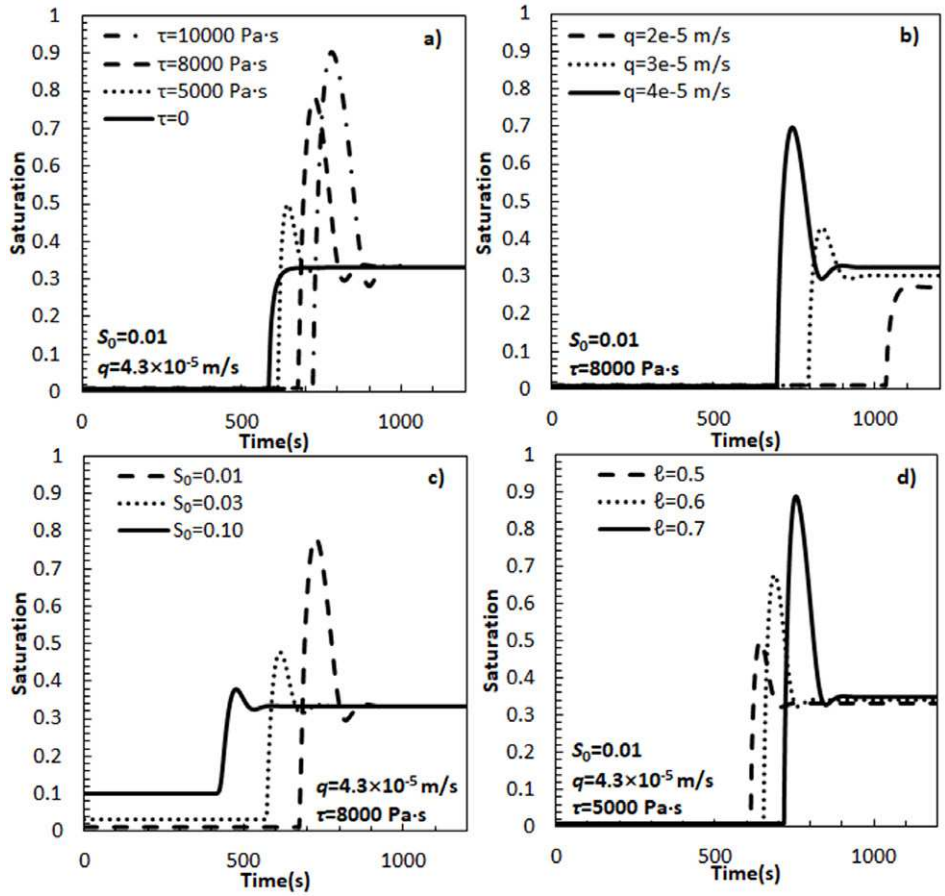

Fig. 5. Saturation breakthrough curves obtained using the extended-standard (ESD) model with different values of the parameters (a) τ, (b) inflow rate (q), (c) initial saturation (S_0), and (d) the van Genuchten empirical parameter l. No hysteresis was included.

a series of simulations with the inflow rate ranging from 2×10^{-5} to 4×10^{-5} m s^{-1} (see Fig. 5b) and with the initial saturation varying from 0.01 to and 0.10 (see Fig. 5c). For a constant τ value, reducing the inflow rate leads to less saturation overshoot (Fig. 5b). For the smallest flow rate of 4×10^{-5} m s^{-1}, the saturation overshoot even vanished. This result was also demonstrated mathematically by van Duijn et al. (2018). As shown in Fig. 5c, the increase in initial saturation resulted in earlier arrival of the front and less saturation overshoot, consistent with the experiments. We also varied the value of the exponent l in the relative permeability, Eq. [4]. Results are shown in Fig. 5d. Decreasing the relative permeability k^{rw} (i.e., increasing the value of the exponent l) leads to more saturation overshoot and later arrival of the moisture front, similar to the effect of τ.

We also did a sensitivity analysis for the ESD model considering capillary hysteresis and the IFA model. A similar trend was found as shown here, except for different shapes of the saturation overshoot. For this reason, we present next the shapes of saturation overshoot obtained with the ESD and IFA models. We studied the effects of including hysteresis in the capillary pressure p^c and/or relative permeability k^{rw}. Figure 6a shows saturation breakthrough curves obtained with the ESD model. As can be seen, including hysteresis had no effect on the results if τ = 0. The reason is that when τ = 0, a monotonic saturation distribution will be obtained, which means that the domain will undergo imbibition only. For τ = 10,000 Pa s, a sharp saturation overshoot results when hysteresis is not included (the same curve as in Fig. 5a). When we accounted for hysteresis in capillary pressure and/or relative permeability, the overshoot showed a plateau (see Fig. 6a).

Finally, we compared the ESD model (with hysteresis) with the IFA model. Typical results are shown in Fig. 6b. The three breakthrough curves for the ESD model are the same as those in Fig. 6a (with τ = 10,000 Pa s). The IFA model (using a p^c–S^w–a^{wa} surface with the imbibition k^{rw}–S^w curve) showed a sharp overshoot. We still obtained a sharp overshoot even if a k^{rw}–S^w–a^{wa} surface was used (i.e., to account for hysteresis in k^{rw}). However, the overshoot height decreased and the front arrived earlier. This is because we effectively allowed for a higher relative permeability value during the imbibition stage when hysteresis was considered.

The difference in results obtained with the ESD and IFA models can be explained partly by differences in the scanning curves implicit in the two models. Figure 7 shows the scanning curves for capillary pressure corresponding to breakthrough curves at x = 20 cm (results shown in Fig. 6b). The solid and dashed lines are primary imbibition and main drainage curves, respectively, as obtained experimentally. In the simulations, saturation at x = 20 cm started from initial saturation and increased along the primary imbibition curve until the front passed. Then saturation

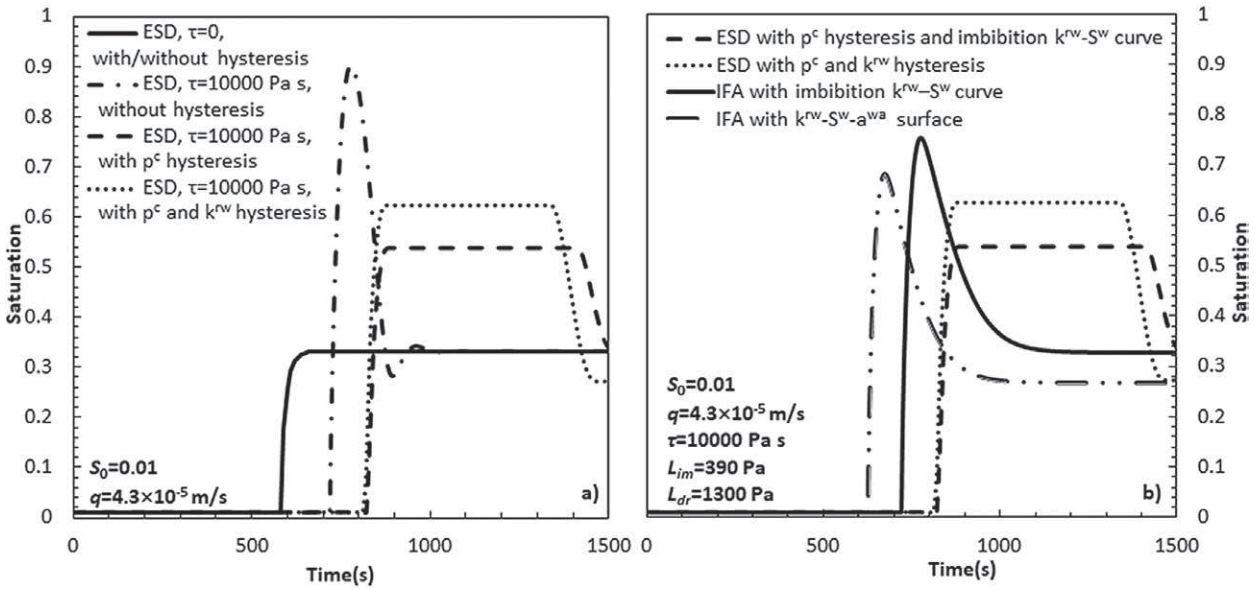

Fig. 6. Saturation breakthrough curves obtained with (a) the extended-standard (ESD) model and (b) the interfacial area (IFA) model (q, inflow rate; S_0, initial saturation; τ, dynamic capillarity coefficient; L_{im} and L_{dr}, defined in Eq. [17]). Hysteresis was included.

decreased along a drainage scanning curve, which is a vertical line as we used for the play-type hysteresis model. This is why the ESD model produces a plateau. If we had used a hysteresis model with a non-vertical scanning curve, the plateau would have a slope. Once the main drainage curve is reached, saturation decreases fast and reaches a steady-state finger saturation. As the finger arrives, a path is followed on the p^c–S^w–a^{wa} surface. The projection of that path on the p^c–S^w plane results in a "primary imbibition curve" shown by the + symbols in Fig. 7b. This path is almost parallel to the primary imbibition curve that was measured.

Our findings suggest that the construction of the p^c–S^w–a^{wa} surface agrees quite well with the measured p^c–S^w imbibition curve. Note that the p^c–S^w–a^{wa} surface used in the IFA model was fitted based on static p^c–S^w–a^{wa} "data" points (generated using the method in Appendix A). However, paths followed on the surface during transient imbibition or drainage are controlled by the coefficients L_{im} and L_{dr}. Due to the lack of studies on these parameters, we chose to fit the two values based on the saturation overshoot experimental data, assuming constant values. However, these parameters are material properties and could be a function of the saturation and/or the interfacial area. That dependence may help to get a better agreement of the path with the measured imbibition curve. As the front passes and saturation starts to decrease, the projection of the path on the p^c–S^w–a^{wa} surface onto the p^c–S^w plane produces the scanning curve shown in Fig. 7b (diamond symbols). Note that this is a transient scanning curve, very different from the "static" scanning curves.

Comparison of Simulation Results with Experiments

Next, we used the two models to simulate the experiments. Parameter values for the ESD model (τ) and the IFA model (τ, L_{im}, and L_{dr}) were fitted first to match a measured breakthrough curve (for the experiment with an inflow rate of 4.3×10^{-5} m s^{-1}) as closely as possible. The fitted values for L_{im} and L_{dr} were fixed subsequently to simulate other experiments with different conditions. Hence only one parameter (τ in both the IFA and ESD models)

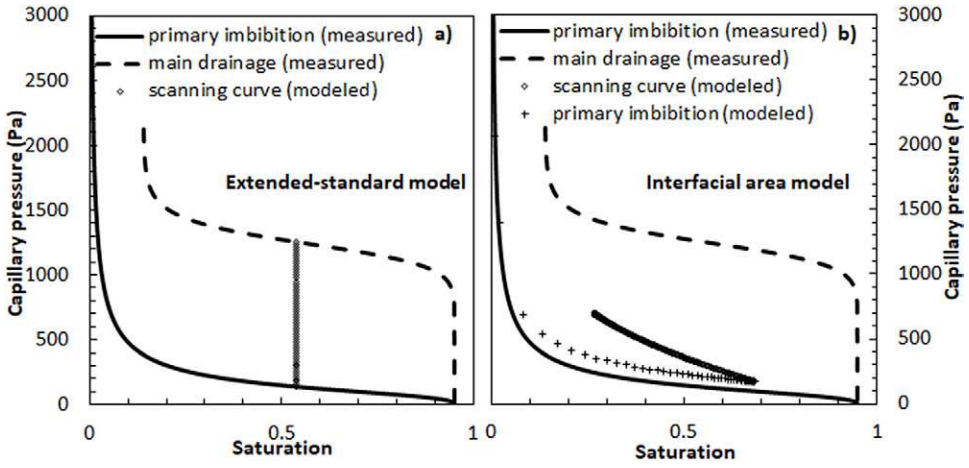

Fig. 7. Pressure–saturation curves corresponding to (a) the extended-standard (ESD) model and (b) the interfacial area (IFA) model.

was fitted to the data. The inflow rate q for the interfacial area model was slightly adjusted as well to fit the correct arrival time of saturation overshoot as measured in the experiments.

The simulated and experimental results are both shown in Fig. 8. We simulated the experiments for three different inflow rates (of the six flow rates considered). Experimental data are shown by symbols, while simulation results from the ESD and IFA models are presented by dashed and solid lines, respectively. Values of all fitting parameters in the simulations are given in Table 3. The results obtained with the ESD model deviated substantially from the data, while the results from the IFA model showed much better agreement. The fitted values of L_{im} and L_{dr} are different from those of Zhuang et al. (2017b) but have the same order of magnitude. Because L is a material property, different values may reasonably be expected for different sands.

We also performed simulations using the Kool–Parker hysteresis model (Kool and Parker, 1987), while still including the dynamic capillarity term. However, the shape of saturation overshoot was quite similar to the overshoot using the play-type hysteresis. The simulation results using Kool–Parker hysteresis are provided in the Supplemental Material.

Summary and Conclusions

This study involved a series of quasi-one-dimensional water infiltration experiments. Clean sand was packed uniformly at three different saturations (0.00, 0.03, and 0.10) in a very narrow acrylic plastic column (1 cm in diameter, 50 cm in length). Water was applied at the top of the column at a constant flow rate. Six different flow rates were used in different experiments. Saturation was measured at a position 20 cm below the inlet. Saturation overshoot was observed for the experiments with initial saturations of 0.00 and 0.03 for all imposed flow rates. However, saturation overshoot did not occur in the experiment with the initial saturation at 0.10.

Two different unsaturated flow models were used to simulate the experiments. For both models, we used the extended Richards equation including a dynamic capillarity term. However, hysteresis was modeled differently. One model, the ESD model, used traditional hysteresis equations for the capillary pressure and relative permeability curves. The other model, the IFA model, used three-dimensional surfaces of p^c–S^w–a^{wa} and k^{rw}–S^w–a^{wa}. To our knowledge, this was the first time a combination of the IFA model and a dynamic capillarity equation was used to simulate a set of experiments.

Without a dynamic capillarity term, completely monotonic saturation profiles were obtained regardless of how hysteresis was included. This result is very much consistent with previous studies. When including a dynamic term, the ESD model gave a sharp saturation overshoot if no hysteresis was included. Accounting for hysteresis in the capillary pressure and/or relative permeability caused the overshoot to produce a plateau structure. The wide

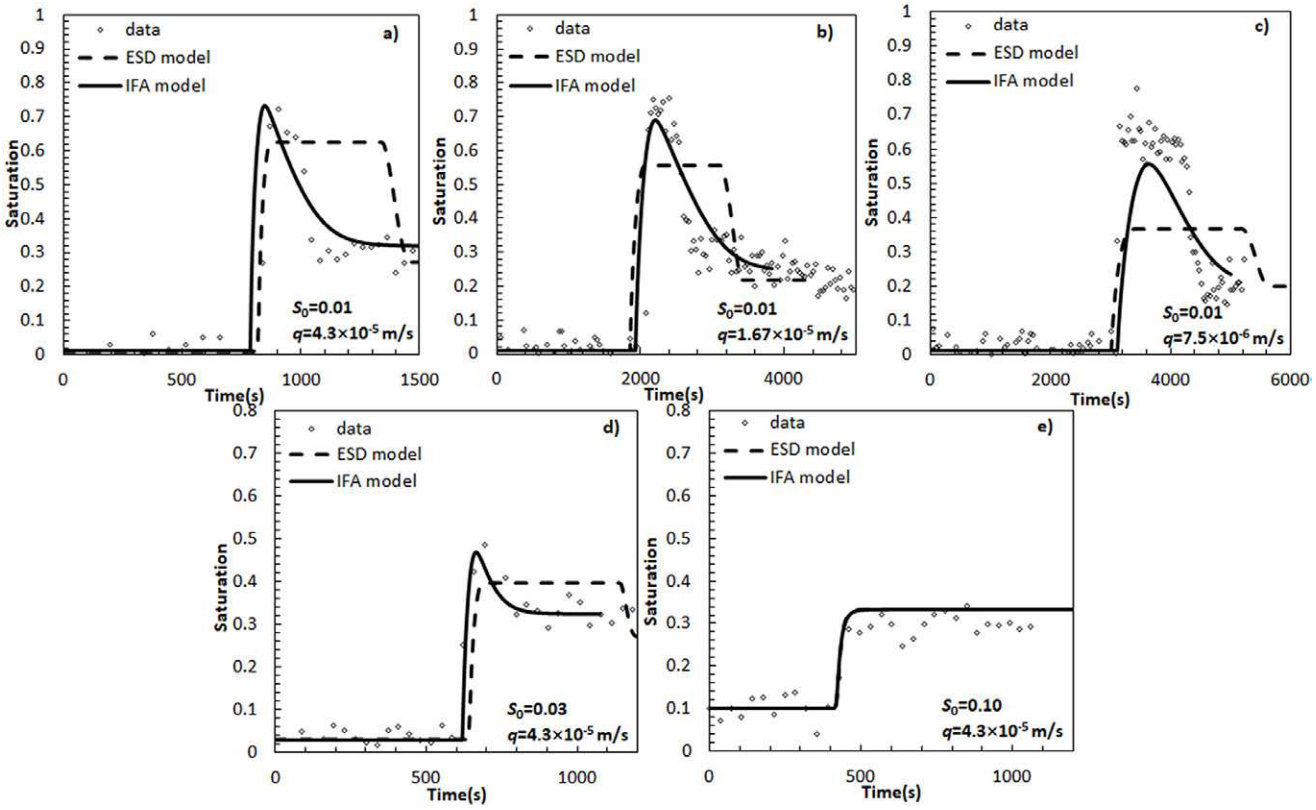

Fig. 8. Observed saturation breakthrough curve at 20 cm (diamonds) and fitted curves obtained with the extended-standard (ESD) model (dashed line) and the interfacial area (IFA) model (solid line) at initial saturation (S_0) of 0.01 and (a) inflow rate (q) of 4.3 × 10^{-5}, (b) 1.67 × 10^{-5}, and (c) 7.5 × 10^{-6} m s^{-1} and at q = 4.3 × 10^{-5} m s^{-1} and initial saturations of (d) 0.03 and (e) 0.10.

(prolonged) saturation overshoot obtained with the ESD model deviated very significantly from the measured data.

The ESD model was not able to reproduce the form of saturation overshoot for any combination of parameter values. The IFA model, on the other hand, could reproduce the saturation overshoots reasonably well, albeit by optimizing the value of the coefficients L_{im} and L_{dr} in the production term. We point out that due to the lack of studies on these two parameters, we decided to assume constant values and to fit them using the saturation overshoot experimental data. However, these parameters in actuality are material properties and may well be a function of saturation and/or interfacial area. Here, we have shown the capability of an alternative approach (the IFA model) to simulate unsaturated flow in porous media. Further investigations are needed, especially experimental studies in conjunction with comprehensive analyses using the ESD and IFA models, to fully understand parameterizations of the production term. For example, the value of dynamic capillarity τ was obtained by fitting both models to the data. Fitted values of τ were found to vary between 10^3 and 2.5×10^5 Pa s, which is consistent with other studies. While in our work we assumed τ to be constant, further studies are needed to determine its dependence on saturation.

Appendix A

Reconstruction of the Interfacial Area Surface

The experiments used for our simulations did not involve measurements of the specific interfacial area. Our assumption was that the projection of the interfacial area surface onto the p^c–S^w plane should provide the full set of curves found in the hysteresis loop. Hence, the inverse reasoning would be that hysteretic capillary pressure curves should give us the p^c–S^w–a^{wa} surface. Ways of estimating the p^c–S^w–a^{wa} surface from p^c–S^w curves have been proposed, among others, by Leverett (1941), Bradford and Leij (1997), and Grant and Gerhard (2007). The underlying assumption is that in quasi-static drainage or imbibition processes, the changes in interfacial area are brought about by mechanical work done (e.g., by fluid pressure) on the system. The magnitude of this mechanical work is related to the area under the p^c–S^w curves.

In an air–water system, the external work needed to effectuate a change $\Delta S^w = -\Delta S^a$ can be written as

$$\Delta W_{ex} = p^a \phi V \Delta S^a + p^w \phi V \Delta S^w = -p^c \phi V \Delta S^w \qquad [A1]$$

where W_{ex} is the external work, V is the bulk volume of the porous medium, and p^a and S^a are the air pressure and air saturation, respectively. Assuming that the solid interface is perfectly wetted by water, the external work will be spent on creating air–water interfaces. The energy associated with changes in the air–water interfaces is

$$\Delta E = \sigma^{wa} \Delta A^{wa} \qquad [A2]$$

which should be equal to ΔW_{ex}. This leads to the following equation for the specific interfacial area $a^{wa} = A^{wa}/V$:

$$a^{wa} = \frac{\phi}{\sigma^{wa}} \int_{S^w}^{1-S_r^a} p_c(z) \mathrm{d}z \qquad [A3]$$

where σ^{wa} is the air–water interfacial tension, and z is a dummy variable.

Equation [A3] is only an approximation in that other effects may need to be included (see, e.g., Grant and Gerhard, 2007), but the equation should suffice for the purposes of this study. For the sand used in our experiments, we had measured primary imbibition and main drainage curves, as well as the van Genuchten parameters fitted to the p^c–S^w data. Thus, for any given saturation, a p^c value was available depending on the curve to be considered. For the S^w and p^c (and that curve), Eq. [A3] could also be used to calculate a^{wa}. This would allow generation of a large set of p^c–S^w–a^{wa} data. We chose 50 saturation values with equal intervals, from 0 to 0.95 ($= 1 - S_r^a$) for imbibition and from 0.14 ($= S_{ir}^w$) to 0.95 ($= 1 - S_r^a$) for main drainage. This set of p^c–S^w–a^{wa} data was used to estimate the parameters of the power function given by Eq. [11], thus obtaining the corresponding p^c–S^w–a^{wa} surface for this sand. The corresponding values of relative permeability k^{rw} were calculated based on Eq. [5] for the same set of saturation values. The resulting set of k^{rw}–S^w–a^{wa} values was fitted with Eq. [12] to obtain a k^{rw}–S^w–a^{wa} surface.

Appendix B

Measurement Accuracy of Gamma-Ray System

To determine the measurement accuracy for different measurement durations, we used data from an unsaturated sand in the experimental setup (shown in Fig. 3). We measured the intensity of γ-rays at one location of the setup 10 times at each measuring duration. Different measuring durations were chosen as 5, 10, 20, 30, 50, 100, and 200 s. Standard deviations for different measuring durations are shown in Fig. B1. Because a short measuring duration is preferable to capture the flow dynamics, we chose 20 s as the measuring duration for the experiments.

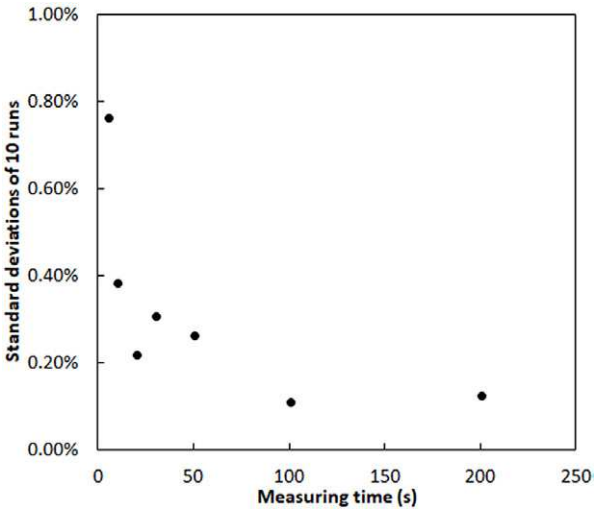

Fig. B1. Standard deviations of the γ-ray data for different measuring durations.

Acknowledgments

We would like to thank M.Th. van Genuchten for his comments on the manuscript. This work was carried out in collaboration with the Darcy Center. S.M.H. received funding from the European Research Council under the European Union's Seventh Framework Program (FP/2007-2013)/ERC Grant Agreement no. 341225. We would like to thank Associate Editor Asim Biswas and two anonymous reviewers for providing comments on the manuscript.

References

Abidoye, L.K., and D.B. Das. 2014. Scale dependent dynamic capillary pressure effect for two-phase flow in porous media. Adv. Water Resour. 74:212–230. doi:10.1016/j.advwatres.2014.09.009

Bauters, T.W., D. DiCarlo, T. Steenhuis, and J.-Y. Parlange. 2000. Soil water content dependent wetting front characteristics in sands. J. Hydrol. 231–232:244–254. doi:10.1016/S0022-1694(00)00198-0

Beliaev, A.Y., and S.M. Hassanizadeh. 2001. A theoretical model of hysteresis and dynamic effects in the capillary relation for two-phase flow in porous media. Transp. Porous Media 43:487–510. doi:10.1023/A:1010736108256

Bottero, S., S.M. Hassanizadeh, P.J. Kleingeld, and T.J. Heimovaara. 2011. Nonequilibrium capillarity effects in two-phase flow through porous media at different scales. Water Resour. Res. 47:W10505. doi:10.1029/2011WR010887

Bradford, S.A., and F.J. Leij. 1997. Estimating interfacial areas for multi-fluid soil systems. J. Contam. Hydrol. 27:83–105. doi:10.1016/S0169-7722(96)00048-4

Brooks, R., and A. Corey. 1964. Hydraulic properties of porous media. Hydrol. Pap. 3. Colorado State Univ., Fort Collins.

Cao, X., and I.S. Pop. 2016. Degenerate two-phase porous media flow model with dynamic capillarity. J. Differ. Equ. 260:2418–2456. doi:10.1016/j.jde.2015.10.008

Chen, L., and T.C.G. Kibbey. 2006. Measurement of air–water interfacial area for multiple hysteretic drainage curves in an unsaturated fine sand. Langmuir 22:6874–6880. doi:10.1021/la053521e

Chen, D., L.J. Pyrak-Nolte, J. Griffin, and N. J. Giordano. 2007. Measurement of interfacial area per volume for drainage and imbibition. Water Resour. Res. 43:W12504. doi:10.1029/2007WR006021

COMSOL. 2014. COMSOL Multiphysics 5.0. COMSOL Inc., Burlington, MA.

Cuesta, C., and J. Hulshof. 2003. A model problem for groundwater flow with dynamic capillary pressure: Stability of travelling waves. Nonlinear Anal. 52:1199–1218. doi:10.1016/S0362-546X(02)00160-8

Cueto-Felgueroso, L., and R. Juanes. 2008. Nonlocal interface dynamics and pattern formation in gravity-driven unsaturated flow through porous media. Phys. Rev. Lett. 101:244504. doi:10.1103/PhysRevLett.101.244504

Das, D.B., and M. Mirzaei. 2012. Dynamic effects in capillary pressure relationships for two-phase flow in porous media: Experiments and numerical analyses. AIChE J. 58:3891–3903. doi:10.1002/aic.13777

Diamantopoulos, E., and W. Durner. 2012. Dynamic nonequilibrium of water flow in porous media: A review. Vadose Zone J. 11(3). doi:10.2136/vzj2011.0197

DiCarlo, D.A. 2004. Experimental measurements of saturation overshoot on infiltration. Water Resour. Res. 40:W04215. doi:10.1029/2003WR002670

DiCarlo, D.A. 2005. Modeling observed saturation overshoot with continuum additions to standard unsaturated theory. Adv. Water Resour. 28:1021–1027. doi:10.1016/j.advwatres.2004.12.003

DiCarlo, D.A. 2007. Capillary pressure overshoot as a function of imbibition flux and initial water content. Water Resour. Res. 43:W08402. doi:10.1029/2006WR005550

Diment, G., and K. Watson. 1985. Stability analysis of water movement in unsaturated porous materials: 3. Experimental studies. Water Resour. Res. 21:979–984. doi:10.1029/WR021i007p00979

Egorov, A.G., R.Z. Dautov, J.L. Nieber, and A.Y. Sheshukov. 2002. Stability analysis of traveling wave solution for gravity-driven flow. Dev. Water Sci. 47:121–128. doi:10.1016/S0167-5648(02)80053-3

Egorov, A.G., R.Z. Dautov, J.L. Nieber, and A.Y. Sheshukov. 2003. Stability analysis of gravity-driven infiltrating flow. Water Resour. Res. 39:1266. doi:10.1029/2002WR001886

Eliassi, M., and R.J. Glass. 2002. On the porous-continuum modeling of gravity-driven fingers in unsaturated materials: Extension of standard theory with a hold-back-pile-up effect. Water Resour. Res. 38(11):1234. doi:10.1029/2001WR001131

Fritz, S. 2012. Experimental investigations of water infiltration into unsaturated soil: Analysis of dynamic capillarity effects. M.S. thesis. Stuttgart Univ., Stuttgart, Germany.

Fürst, T., R. Vodák, M. Šír, and M. Bíl. 2009. On the incompatibility of Richards' equation and finger-like infiltration in unsaturated homogeneous porous media. Water Resour. Res. 45:W03408. doi:10.1029/2008WR007062

Geiger, S.L., and D.S. Durnford. 2000. Infiltration in homogeneous sands and a mechanistic model of unstable flow. Soil Sci. Soc. Am. J. 64:460–469. doi:10.2136/sssaj2000.642460x

Glass, R.J., J.-Y. Parlange, and T.S. Steenhuis. 1989a. Wetting front instability: 1. Theoretical discussion and dimensional analysis. Water Resour. Res. 25:1187–1194. doi:10.1029/WR025i006p01187

Glass, R.J., T.S. Steenhuis, and J.-Y. Parlange. 1989b. Mechanism for finger persistence in homogeneous, unsaturated, porous media: Theory and verification. Soil Sci. 148:60–70. doi:10.1097/00010694-198907000-00007

Goel, G., L.K. Abidoye, B.R. Chahar, and D.B. Das. 2016. Scale dependency of dynamic relative permeability–saturation curves in relation with fluid viscosity and dynamic capillary pressure effect. Environ. Fluid Mech. 16:945–963. doi:10.1007/s10652-016-9459-y

Grant, G.P., and J.I. Gerhard. 2007. Simulating the dissolution of a complex dense nonaqueous phase liquid source zone: 1. Model to predict interfacial area. Water Resour. Res. 43:W12410. doi:10.1029/2007WR006038

Hassanizadeh, S.M. 2015. Advanced theories of two-phase flow in porous media. In: K. Vafai, editor, Handbook of porous media. 3rd ed. CRC Press, Boca Raton, FL. p. 47–62.

Hassanizadeh, S.M., M.A. Celia, and H.K. Dahle. 2002. Dynamic effect in the capillary pressure–saturation relationship and its impacts on unsaturated flow. Vadose Zone J. 1:38–57. doi:10.2136/vzj2002.3800

Hassanizadeh, S.M., and W.G. Gray. 1990. Mechanics and thermodynamics of multiphase flow in porous media including interphase boundaries. Adv. Water Resour. 13:169–186. doi:10.1016/0309-1708(90)90040-B

Hassanizadeh, S.M., and W.G. Gray. 1993a. Thermodynamic basis of capillary pressure in porous media. Water Resour. Res. 29:3389–3405. doi:10.1029/93WR01495

Hassanizadeh, S.M., and G.W. Gray. 1993b. Toward an improved description of the physics of two-phase flow. Adv. Water Resour. 16:53–67. doi:10.1016/0309-1708(93)90029-F

Held, R.J., and M.A. Celia. 2001. Modeling support of functional relationships between capillary pressure, saturation, interfacial area and common lines. Adv. Water Resour. 24:325–343. doi:10.1016/S0309-1708(00)00060-9

Hill, D.E., and J.-Y. Parlange. 1972. Wetting front instability in layered soils. Soil Sci. Soc. Am. J. 36:697–702. doi:10.2136/sssaj1972.03615995003600050010x

Hilpert, M. 2012. Velocity-dependent capillary pressure in theory for variably-saturated liquid infiltration into porous media. Geophys. Res. Lett. 39:L06402. doi:10.1029/2012GL051114

Joekar-Niasar, V., and S.M. Hassanizadeh. 2011a. Specific interfacial area: The missing state variable in two-phase flow equations? Water Resour. Res. 47:W05513. doi:10.1029/2010WR009291

Joekar-Niasar, V., and S.M. Hassanizadeh. 2011b. Effect of fluids properties on non-equilibrium capillarity effects: Dynamic pore-network modeling. Int. J. Multiphase Flow 37:198–214. doi:10.1016/j.ijmultiphaseflow.2010.09.007

Joekar-Niasar, V., and S.M. Hassanizadeh. 2012. Uniqueness of specific interfacial area–capillary pressure–saturation relationship under non-equilibrium conditions in two-phase porous media flow. Transp. Porous Media 94:465–486. doi:10.1007/s11242-012-9958-3

Joekar-Niasar, V., S.M. Hassanizadeh, and A. Leijnse. 2008. Insights into the

relationships among capillary pressure, saturation, interfacial area and relative permeability using pore-network modeling. Transp. Porous Media 74:201–219. doi:10.1007/s11242-007-9191-7

Jury, W.A., Z. Wang, and A. Tuli. 2003. A conceptual model of unstable flow in unsaturated soil during redistribution. Vadose Zone J. 2:61–67. doi:10.2136/vzj2003.6100

Kalaydjian, F. 1987. A macroscopic description of multiphase flow in porous media involving spacetime evolution of fluid/fluid interface. Transp. Porous Media 2:537–552. doi:10.1007/BF00192154

Karadimitriou, N.K., S.M. Hassanizadeh, V. Joekar-Niasar, and P.J. Kleingeld. 2014. Micromodel study of two-phase flow under transient conditions: Quantifying effects of specific interfacial area. Water Resour. Res. 50:8125–8140. doi:10.1002/2014WR015388

Kool, J.B., and J.C. Parker. 1987. Development and evaluation of closed-form expressions for hysteretic soil hydraulic properties. Water Resour. Res. 23:105–114. doi:10.1029/WR023i001p00105

Landa-Marbán, D., F.A. Radu, and J.M. Nordbotten. 2017. Modeling and simulation of microbial enhanced oil recovery including interfacial area. Transp. Porous Media 120:395–413. doi:10.1007/s11242-017-0929-6

Leverett, M. 1941. Capillary behavior in porous solids. Trans. AIME 142:152–169. doi:10.2118/941152-G

Liu, Y., T.S. Steenhuis, and J.-Y. Parlange. 1994a. Formation and persistence of fingered flow fields in coarse grained soils under different moisture contents. J. Hydrol. 159:187–195. doi:10.1016/0022-1694(94)90255-0

Liu, Y., T.S. Steenhuis, and J.-Y. Parlange. 1994b. Closed-form solution for finger width in sandy soils at different water contents. Water Resour. Res. 30:949–952. doi:10.1029/94WR00068

Luckner, L., M.Th. van Genuchten, and D.R. Nielsen. 1989. A consistent set of parametric models for the two-phase flow of immiscible fluids in the subsurface. Water Resour. Res. 25:2187–2193. doi:10.1029/WR025i010p02187

Manthey, S., S.M. Hassanizadeh, R. Helmig, and R. Hilfer. 2008. Dimensional analysis of two-phase flow including a rate-dependent capillary pressure–saturation relationship. Adv. Water Resour. 31:1137–1150. doi:10.1016/j.advwatres.2008.01.021

Nieber, J.L. 1996. Modeling finger development and persistence in initially dry porous media. Geoderma 70:207–229. doi:10.1016/0016-7061(95)00086-0

Nieber, J., A. Sheshukov, A. Egorov, and R. Dautov. 2003. Non-equilibrium model for gravity-driven fingering in water repellent soils: Formulation and 2D simulations. In: C.J. Ritsema and L.W. Dekker, editors, Soil water repellency: Occurrence, consequences, and amelioration. Elsevier, Amsterdam. p. 245–257.

Niessner, J., and S.M. Hassanizadeh. 2008. A model for two-phase flow in porous media including fluid–fluid interfacial area. Water Resour. Res. 44:W08439. doi:10.1029/2007WR006721

Niessner, J., and S.M. Hassanizadeh. 2009a. Non-equilibrium interphase heat and mass transfer during two-phase flow in porous media: Theoretical considerations and modeling. Adv. Water Resour. 32:1756–1766. doi:10.1016/j.advwatres.2009.09.007

Niessner, J., and S.M. Hassanizadeh. 2009b. Modeling kinetic interphase mass transfer for two-phase flow in porous media including fluid–fluid interfacial area. Transp. Porous Media 80:329–344. doi:10.1007/s11242-009-9358-5

O'Carroll, D.M., T.J. Phelan, and L.M. Abriola. 2005. Exploring dynamic effects in capillary pressure in multistep outflow experiments. Water Resour. Res. 41:W11419. doi:10.1029/2005WR004010

Otto, F. 1997. L^1-contraction and uniqueness for unstationary saturated–unsaturated porous media flow. Adv. Math. Sci. Appl. 7:537–553.

Parker, J.C., and R.J. Lenhard. 1987. A model for hysteretic constitutive relations governing multiphase flow: 1. Saturation–pressure relations. Water Resour. Res. 23:2187–2196. doi:10.1029/WR023i012p02187

Pop, I.S., C.J. van Duijn, J. Niessner, and S.M. Hassanizadeh. 2009. Horizontal redistribution of fluids in a porous medium: The role of interfacial area in modeling hysteresis. Adv. Water Resour. 32:383–390. doi:10.1016/j.advwatres.2008.12.006

Rätz, A., and B. Schweizer. 2014. Hysteresis models and gravity fingering in porous media. Z. Angew. Math. Mech. 94:645–654. doi:10.1002/zamm.201200052

Reeves, P.C., and M.A. Celia. 1996. A functional relationship between capillary pressure, saturation, and interfacial area as revealed by a pore-scale network model. Water Resour. Res. 32:2345–2358. doi:10.1029/96WR01105

Rezanezhad, F., H. Vogel, and K. Roth. 2006. Experimental study of fingered flow through initially dry sand. Hydrol. Earth Syst. Sci. Discuss. 3:2595–2620. doi:10.5194/hessd-3-2595-2006

Sander, G.C., O.J. Glidewell, and J. Norbury. 2008. Dynamic capillary pressure, hysteresis and gravity-driven fingering in porous media. J. Phys. Conf. Ser. 138:012023. doi:10.1088/1742-6596/138/1/012023

Schweizer, B. 2012. Instability of gravity wetting fronts for Richards equations with hysteresis. Interfaces Free Bound. 14:37–64. doi:10.4171/IFB/273

Selker, J., J.-Y. Parlange, and T. Steenhuis. 1992. Fingered flow in two dimensions: 2. Predicting finger moisture profile. Water Resour. Res. 28:2523–2528. doi:10.1029/92WR00962

Smiles, D.E., G. Vachaud, and M. Vauclin. 1971. A test of the uniqueness of the soil moisture characteristic during transient, nonhysteretic flow of water in a rigid soil. Soil Sci. Soc. Am. J. 35:534–539. doi:10.2136/sssaj1971.03615995003500040018x

Stauffer, F. 1978. Time dependence of the relations between capillary pressure, water content and conductivity during drainage of porous media. In: IAHR symposium on scale effects in porous media, Thessaloniki, Greece. 29 Aug.–1 Sept. 1978. p. 3–35.

Stonestrom, D.A., and K.C. Akstin. 1994. Nonmonotonc matric pressure histories during constant flux infiltration into homogeneous profiles. Water Resour. Res. 30:81–91. doi:10.1029/93WR02476

Topp, G., and A. Peters. 1967. Comparison of water content–pressure head data obtained by equilibrium, steady-state, and unsteady-state methods. Soil Sci. Soc. Am. J. 31:312–314. doi:10.2136/sssaj1967.03615995003100030009x

van Duijn, C.J., Y. Fan, L.A. Peletier, and I.S. Pop. 2013. Travelling wave solutions for degenerate pseudo-parabolic equations modelling two-phase flow in porous media. Nonlinear Anal. Real World Appl. 14:1361–1383. doi:10.1016/j.nonrwa.2012.10.002

van Duijn, C.J., K. Mitra, and I.S. Pop. 2018. Travelling wave solutions for the Richards equation incorporating non-equilibrium effects in the capillarity pressure. Nonlinear Anal. Real World Appl. 41:232–268. doi:10.1016/j.nonrwa.2017.10.015

van Duijn, C.J., L.A. Peletier, and I.S. Pop. 2007. A new class of entropy solutions of the Buckley–Leverett equation. SIAM J. Math. Anal. 39:507–536. doi:10.1137/05064518X

van Duijn, C.J., G.J.M. Pieters, and P.A.C. Raats. 2004. Steady flows in unsaturated soils are stable. Transp. Porous Media 57:215–244. doi:10.1023/B:TIPM.0000038250.72364.20

van Genuchten, M.Th. 1980. A closed-form equation for predicting the hydraulic conductivity of unsaturated soils. Soil Sci. Soc. Am. J. 44:892–898. doi:10.2136/sssaj1980.03615995004400050002x

Wang, Z., J. Feyen, and E.D. Elrick. 1998. Prediction of fingering in porous media. Water Resour. Res. 34:2183–2190. doi:10.1029/98WR01472

Wang, Z., W.A. Jury, A. Tuli, and D.J. Kim. 2004. Unstable flow during redistribution: Controlling factors and practical implications. Vadose Zone J. 3:549–559. doi:10.2136/vzj2004.0549

Xiong, Y. 2014. Flow of water in porous media with saturation overshoot: A review. J. Hydrol. 510:353–362. doi:10.1016/j.jhydrol.2013.12.043

Zhuang, L., S.M. Hassanizadeh, P.J. Kleingeld, and M.Th. van Genuchten. 2017a. Revisiting the horizontal redistribution of water in soils: Experiments and numerical modeling. Water Resour. Res. 53:7576–7589. doi:10.1002/2017WR020410

Zhuang, L., S.M. Hassanizadeh, C.-Z. Qin, and A. de Waal. 2017b. Experimental investigation of hysteretic dynamic capillarity effect in unsaturated flow. Water Resour. Res. 53:9078–9088. doi:10.1002/2017WR020895

Zhuang, L., S.M. Hassanizadeh, M.Th. van Genuchten, A. Leijnse, A. Raoof, and C. Qin. 2016. Modeling of horizontal water redistribution in an unsaturated soil. Vadose Zone J. 15(3). doi:10.2136/vzj2015.08.0109